Why some interfaces cannot be sharp

NAOYUKI NAKAGAWA[1,2], HAROLD Y. HWANG[1,2] AND DAVID A. MULLER[3]*

[1]Department of Advanced Materials Science, University of Tokyo, Kashiwa, Chiba 277-8561, Japan
[2]Japan Science and Technology Agency, Kawaguchi 332-0012, Japan
[3]School of Applied and Engineering Physics, Cornell University, Ithaca, New York 14583, USA
*e-mail: davidm@ccmr.cornell.edu

Published online: 22 January 2006; doi:10.1038/nmat1569

A central goal of modern materials physics and nanoscience is the control of materials and their interfaces to atomic dimensions. For interfaces between polar and nonpolar layers, this goal is thwarted by a polar catastrophe that forces an interfacial reconstruction. In traditional semiconductors, this reconstruction is achieved by an atomic disordering and stoichiometry change at the interface, but a new option is available in multivalent oxides: if the electrons can move, the atoms do not have to. Using atomic-scale electron energy loss spectroscopy, we have examined the microscopic distribution of charge and ions across the (001) $LaAlO_3/SrTiO_3$ interface. We find that there is a fundamental asymmetry between the ionically compensated $AlO_2/SrO/TiO_2$ interface, and the electronically compensated $AlO_2/LaO/TiO_2$ interface, both in interfacial sharpness and charge density. This suggests a general strategy to design sharp interfaces, remove interfacial screening charges, control the band offset and, hence, markedly improve the performance of oxide devices.

Oxide thin films have already found a variety of industrial applications ranging from mainstream electronics to niche markets such as high-frequency filters. The wide variety of ground states available to the oxide family offers the potential for richer functionality than available with the present conventional semiconductors: from piezoelectric resonators to magneto-optical storage. In some cases, atomic-layer control of the growth is possible, presenting opportunities to couple different physical properties at the microscopic level. Several studies have demonstrated that, when interface effects dominate, the structure and stability at small lengthscales introduces a host of new considerations[1–5].

Electrostatic boundary conditions can be a dominant factor controlling the atomic and electronic structure at solid–solid interfaces. Even interfaces between formally neutral planes can have interface dipoles resulting from band offsets and bond polarizations[6,7]. However, for materials with considerable ionic character, polar discontinuities introduce a larger energy cost for atomically abrupt heterointerfaces between planes of different polarity. This is the interface analogue of the divergent surface energy that would result from terminating a material along a polar plane with no surface reconstruction. The consequence for growing polar materials on nonpolar substrates (such as GaAs on Si or Ge) is a catastrophic roughening during growth, unless the composition is graded at the interface to ensure there is no net formal interface charge[8]. This grading results in a microscopically rough interface and, in many cases, also a measurable electrical band offset[8,9].

How the system responds to this energy cost will have consequences for both its electrical and physical properties, such as the creation of interface phases[4,5,10] or differing interface roughness as a function of interface terminations. Much of this behaviour can be captured by a simple electrostatic model, which we discuss and test experimentally for (001) interfaces between $SrTiO_3$, the workhorse oxide semiconductor, and $LaAlO_3$, a closely lattice-matched insulator, useful as a gate dielectric for field-effect devices[11].

THEORY

The (001) planes in the ABO_3 perovskite structure can be divided into alternating layers of AO and BO_2 planes. Taking oxygen to

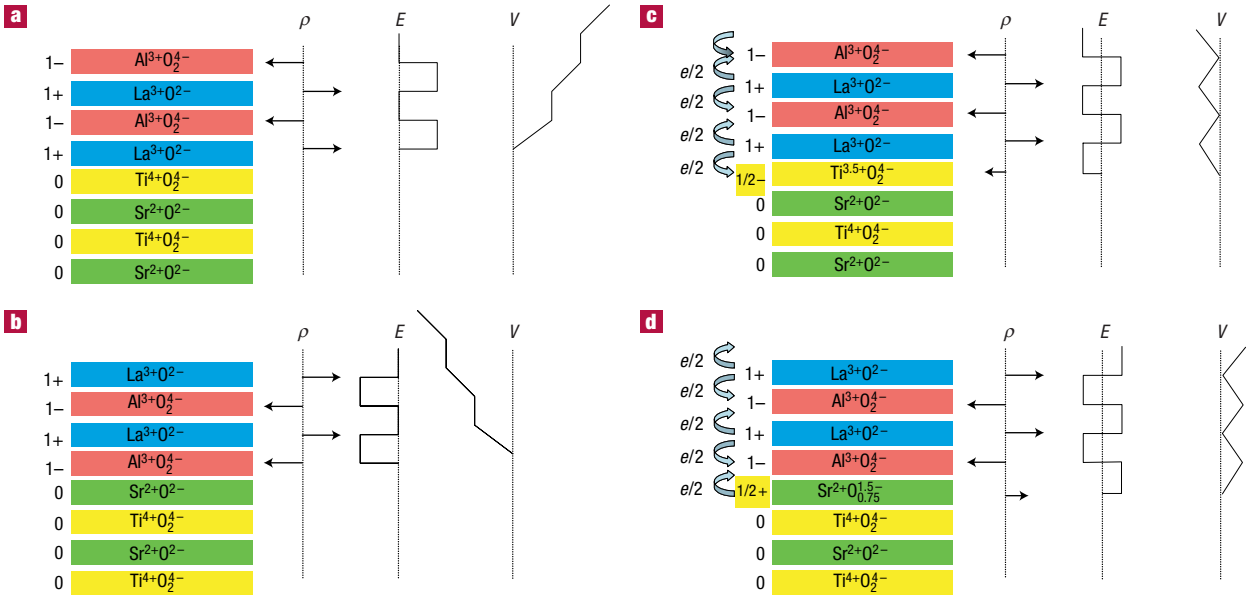

Figure 1 The polar catastrophe illustrated for atomically abrupt (001) interfaces between $LaAlO_3$ and $SrTiO_3$. a, The unreconstructed interface has neutral (001) planes in $SrTiO_3$, but the (001) planes in $LaAlO_3$ have alternating net charges (ρ). If the interface plane is AlO_2/LaO/TiO_2, this produces a non-negative electric field (E), leading in turn to an electric potential (V) that diverges with thickness. **b**, If the interface is instead placed at the AlO_2/SrO/TiO_2 plane, the potential diverges negatively. **c**, The divergence catastrophe at the AlO_2/LaO/TiO_2 interface can be avoided if half an electron is added to the last Ti layer. This produces an interface dipole that causes the electric field to oscillate about 0 and the potential remains finite. The upper free surface is not shown, but in this simple model the uppermost AlO_2 layer would be missing half an electron, which would bring the electric field and potential back to zero at the upper surface. The actual surface reconstruction is more complicated[21]. **d**, The divergence for the AlO_2/SrO/TiO_2 interface can also be avoided by removing half an electron from the SrO plane in the form of oxygen vacancies.

have a formal valence of O^{2-}, the A and B cations can take on values of $A^{4+}B^{2+}$, $A^{3+}B^{3+}$, $A^{2+}B^{4+}$ or $A^{1+}B^{5+}$, such that the ABO_3 bulk structure remains neutral. Fractional charge values also arise from solid solutions and/or mixed valence states. Just as compound semiconductors made from group IV elements such as Si or Ge have formally neutral (001) planes, the $A^{2+}B^{4+}O_3$ or 'II–IV' structure (such as $SrTiO_3$) also contains neutral AO and BO_2 (001) planes. An analogue of the III–V or II–VI semiconductors such as GaN or CdTe that have polar planes is the $A^{3+}B^{3+}O_3$ or 'III–III' structure (such as $LaTiO_3$ or $LaAlO_3$), which is composed of +1 AO and −1 BO_2 planes.

If we consider joining perovskites from two different charge families with atomic abruptness in an (001) orientation, a polar discontinuity results at the interface. Taking the example of joining $LaAlO_3$ with $SrTiO_3$, two configurations arise, which can be defined by the composition of the layer between AlO_2 and TiO_2 at the interface: AlO_2/LaO/TiO_2 or AlO_2/SrO/TiO_2. Such a junction between polar and nonpolar planes is very common in oxide heterostructures, and the following discussion applies generally to many perovskite interfaces. Figure 1a,b shows how an atomically abrupt interface between polar and neutral layers leads to a polar catastrophe (where the electrostatic potential diverges with thickness) if there is no redistribution of charges at the interface.

Unlike conventional semiconductors where each ion has a fixed valence, in complex oxides compositional roughening is not the only option for charge rearrangement: mixed valence charge compensation can occur if electrons can be redistributed at lower energy cost than redistributing ions. Conceptually, one can first construct the interface from neutral atoms and then allow ionization, resulting in the net transfer of half an electron per two-dimensional unit cell (e^-/u.c.) from $LaAlO_3$ to $SrTiO_3$ across the interface (Fig. 1c). This process leaves the overall structure neutral, with the Ti ion at the interface becoming $Ti^{3.5+}$, and the potential no longer diverges. The extra half an electron at the AlO_2/LaO/TiO_2 ('n-type') interface should be physically detectable by transport and direct spectroscopic measurements. Indeed, metallic conductivity and Hall measurements suggest free electrons at the n-type interface[10]. Figure 1d shows the analogous construction for the AlO_2/SrO/TiO_2 interface where the SrO layer must now acquire an extra half a hole per two-dimensional unit cell (e^+/u.c.) to maintain charge neutrality, that is, formally it should be 'p-type'. Electrically, however, this interface is insulating[10]. As this positive charge is still electrostatically necessary to avoid the divergence, and there are no available mixed-valence states to compensate for the half a hole (such as $Ti^{4.5+}$, which is energetically inaccessible), an atomic reconstruction is required.

Here we show direct experimental evidence that the induced interface charges at the AlO_2/LaO/TiO_2 interfaces are compensated for by mixed-valence Ti states that place extra electrons in the $SrTiO_3$ conduction band. In contrast to this electronic interface reconstruction, the AlO_2/SrO/TiO_2 interface is compensated by the introduction of oxygen vacancies at the interface, an atomic interface reconstruction. For repeated growth of polar interfaces in $LaAlO_3$/$SrTiO_3$ superlattices, the cations intermix rapidly to reduce the interface dipole energy, representing a fundamental limit on the growth stability of multiple polar interfaces.

RESULTS

To understand the electrical asymmetry between the two interface terminations, we examined the interfaces with atomic-resolution electron energy loss spectroscopy (EELS) performed in a scanning transmission electron microscope (STEM) with single atom and vacancy sensitivity[12,13]. Atomic-scale measurements of composition

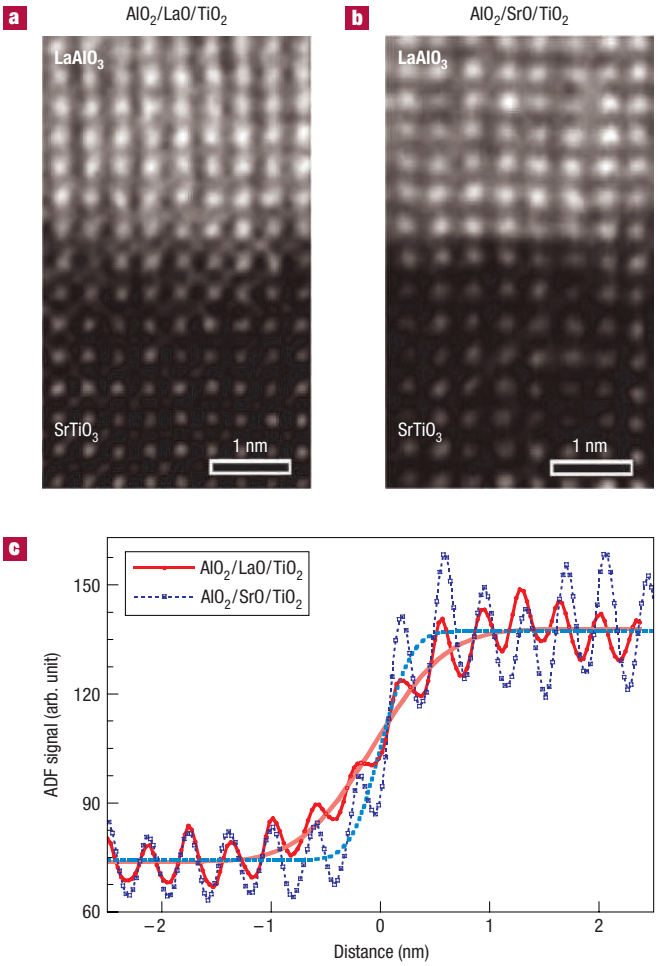

Figure 2 ADF-STEM images of the interface structures. La ions are brightest, followed by Sr, with the Ti occasionally faintly visible in between (the contrast is insufficient to resolve the Al or O ions). **a**, $LaAlO_3$ grown on TiO_2-terminated $SrTiO_3$ (forming the $AlO_2/LaO/TiO_2$ interface). **b**, $LaAlO_3$ grown on SrO-terminated $SrTiO_3$ (forming the $AlO_2/SrO/TiO_2$ interface). **c**, Averaged line profiles across the interfaces of **a**,**b**. An error-function curve is fit to both profiles to extract the average interface width. After accounting for a 0.2 nm probe size, the r.m.s. roughness for the $AlO_2/LaO/TiO_2$ interface of **a** is $\sigma = 1.90 \pm 0.11$ u.c., and for the $AlO_2/SrO/TiO_2$ interface of **b**, $\sigma = 0.77 \pm 0.13$ u.c.

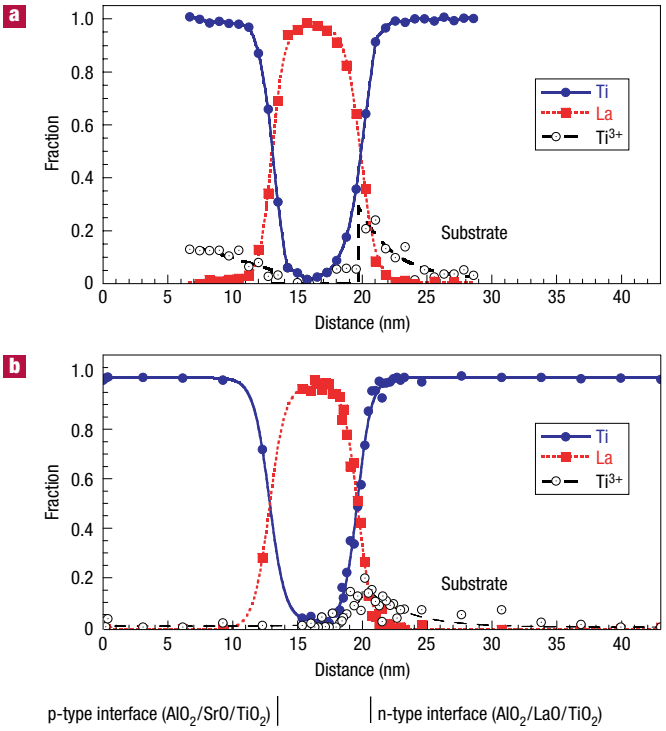

Figure 3 $SrTiO_3/LaAlO_3/SrTiO_3$ multilayer. a, Before and **b**, after annealing. The growth direction is right to left. The lower interface remains metallic and unchanged after annealing. The upper interface was insulating (no Ti^{3+}) before annealing, even though the $SrTiO_3$ layer above it contained oxygen vacancies. After annealing, the vacancies have been filled. Also note from **a** that the upper interface (p-type) is less diffuse than the lower interface (n-type).

and electronic structure at buried interfaces are possible[13–15] using EELS from a high-energy (200 keV) electron beam focused down to a spot as small as 1–3 Å. By passing such a small electron beam through a thinned section, the excited states of atoms in their bulk environment can be probed. Electron-transparent cross-sectioned samples have been prepared by tripod polishing with water-free lubricants, followed by low-energy low-angle ion milling on a liquid-nitrogen-cooled stage. The wedge geometry allows us to examine the interface as a function of sample thickness, thereby separating out potential surface damage from the underlying bulk properties. We collect only small-angle inelastic scattering (<20 mrad), a regime in which the shape of the EELS signal becomes formally equivalent to that obtained from X-ray absorption spectroscopy[16]. The remaining high-angle (>50 mrad) scattering is predominantly elastic, and is used to form a simultaneously recorded annular dark field (ADF) image, with the heaviest atoms appearing the brightest[17].

Figure 2 shows the interface structure of the $LaAlO_3$ films grown on $SrTiO_3$. The structures in this study were grown by pulsed laser deposition in an ultrahigh-vacuum chamber on atomically flat, TiO_2-terminated (001) $SrTiO_3$ single-crystal substrates. $LaAlO_3$, $SrTiO_3$, SrO single crystal targets and $La_2Ti_2O_7$ polycrystalline targets were used for two-dimensional layer-by-layer growth, as monitored by unit-cell reflection high-energy electron diffraction intensity oscillations throughout growth. The structures were grown at 750 °C under an oxygen partial pressure (P_{O_2}) of 1×10^{-5} torr, after pre-annealing the substrate at 960 °C in $P_{O_2} = 5 \times 10^{-6}$ torr for 30 min to removed surface contaminants. The laser spot was formed just off of the focusing condition with an average fluence of 3 J cm^{-2}, operating at a repetition rate of 5 Hz. We find that the $AlO_2/LaO/TiO_2$ interface is twice as rough as the $AlO_2/SrO/TiO_2$ interface (Fig. 2c). Even when the order of growth is switched and $SrTiO_3$ is grown atop $LaAlO_3$, the upper $AlO_2/SrO/TiO_2$ interface is still more abrupt than the lower $AlO_2/LaO/TiO_2$ interface (Fig. 3). Also shown in Fig. 3 is a comparison of as-grown interfaces with those annealed at 550 °C in O_2 for 4 h. In all cases, we found no change in the interface atomic or electronic structure with annealing. The effect of annealing was to fill residual oxygen vacancies in $SrTiO_3$ film layers, as well as improving the crystallinity of the film, therefore data from the annealed interfaces are presented here.

Figure 4a shows that as we continue to grow repeated $LaAlO_3/SrTiO_3$ multilayers, the interface roughness rapidly increases with each added multilayer. These structures were grown after monolayer deposition of SrO, followed by the repeated

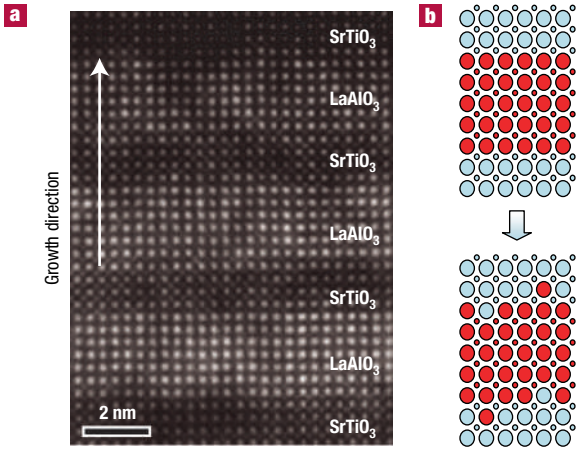

Figure 4 Repeated growth of $LaAlO_3/SrTiO_3$ multilayers. a, A $LaAlO_3/SrTiO_3$ multilayer structure composed of all n-type interfaces shows a progressive increase in interface roughness with growth. **b**, A schematic of the cation intermixing observed in **a**. The large blue circles are Sr, small blue for Ti, large red for La and small red for Al.

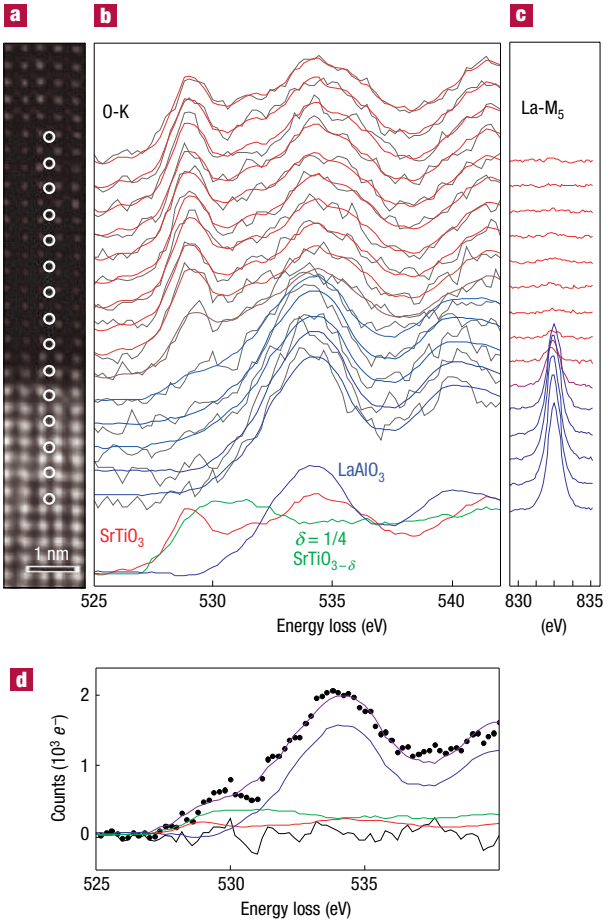

Figure 5 O-K edge EELS profile across a $AlO_2/SrO/TiO_2$ p-type interface. a, The ADF image of the interface: $SrTiO_3$ is the darker material in the upper half of the image and the $LaAlO_3$ film is in the lower half (scale bar 1 nm). **b**, O-K EELS spectra recorded from the circles in **a** (black curves). Bulk reference bulk spectra of O-K edges in $SrTiO_3$ (red curves), $LaAlO_3$ (blue curves) and $\delta = 1/4$ $SrTiO_{3-\delta}$ (green curves) are shown at the bottom of the panel. The coloured lines show least-squares fits to the position-dependent spectra colour-coded by the fractional contribution of the red, green and blue reference spectra. **c**, The La-M edge (simultaneously recorded with the O-K data) showing the interface is graded over 2 u.c. **d**, The bottom panel shows the decomposition of the O-K edge at the interface in detail. Experimental data are shown as black data points, and the violet curve is the fit from the addition of the three reference spectra. The residual to the fit is given by the black curve at the bottom.

growth sequence (1 u.c. of $LaTiO_3$, 4 u.c. of $LaAlO_3$, 4 u.c. of $SrTiO_3$). In this manner, the superlattice is entirely composed of $AlO_2/LaO/TiO_2$ interfaces, hence the insertion of 1 u.c. of $LaTiO_3$ at the leading interface with $LaAlO_3$. By this construction, simple La/Sr interdiffusion cannot remove the polar discontinuity, as illustrated schematically in Fig. 4b.

The microscopic distribution of formal valences is probed using EELS where the Ti-L, O-K and La-M edges are recorded simultaneously. The Ti-L edge provides a useful fingerprint of the Ti^{3+} and Ti^{4+} states from which a Ti *d* electron count and crystal-field symmetry can be extracted by least-squares fit to reference spectra[4,13,18,19]. The O-K edge is also sensitive to the presence of oxygen vacancies and more extended features in the band structure[13,20]. This richness makes it less amenable to an atomistic description. Instead, Fig. 5 shows that for the p-type interface the main features in the O-K edge spectra can be captured by a least-squares fit to reference spectra from bulk $SrTiO_3$, bulk $LaAlO_3$ and oxygen-deficient $SrTiO_{3-\delta}$ with $\delta = 1/4$.

The lack of any statistically significant structure in the residual suggests that at our experimental sensitivity (~5–10%) and resolution (0.7 eV and 0.2 nm), the main changes in the local oxygen-bonding environment at the p-type interface are due to oxygen vacancies. Excluding the oxygen-deficient reference from the fit results in a significant residual, sharply peaked at the interface. EELS line profiles such as those of Fig. 5b were recorded for both interfaces. The integrated Ti, O and La counts give composition profiles, and least-squares fits to the Ti-L and O-K edge data resolve the variations in Ti valence and oxygen occupancy across the interface (see Figs 6 and 3). The quality of the fits can be evaluated from examining the lack of variation in the residuals.

The EELS-derived fractional compositions summarized in Fig. 6 resolve the puzzle over the electrical asymmetry between the n-type $AlO_2/LaO/TiO_2$ and p-type $AlO_2/SrO/TiO_2$ interfaces. We find that for the n-type interface (Fig. 6a), 0.7 ± 0.1 excess e^-/u.c. are found on the Ti sites (non-zero Ti^{3+}) and very few oxygen vacancies (0.1 ± 0.04 V_O/u.c.). There are no excess electrons (0.1 ± 0.1) on the Ti sites for the p-type interface (Fig. 6c), where an extra half a hole would be expected theoretically. Instead, at the $AlO_2/SrO/TiO_2$ interface significant compensating oxygen vacancies (0.32 ± 0.06 V_O/u.c., which would imply 0.64 ± 0.12 fewer electrons at $2e^-$ per O) are present (Fig. 6d), but no free holes are found (which would give a pre-peak on the O-K edge). The EELS measurements suggesting free carriers at the n-type, but not the p-type interface are consistent with the electrical measurements, with the EELS deducing that the sheet carrier density at the n-type interface is close to 5×10^{14} cm^{-2} and confined to within a few nanometres of the interface.

DISCUSSION

The EELS results indicate that accommodation of the polar discontinuity is the driving force for the interface electronic and atomic reconstructions we have observed. Perhaps the most striking

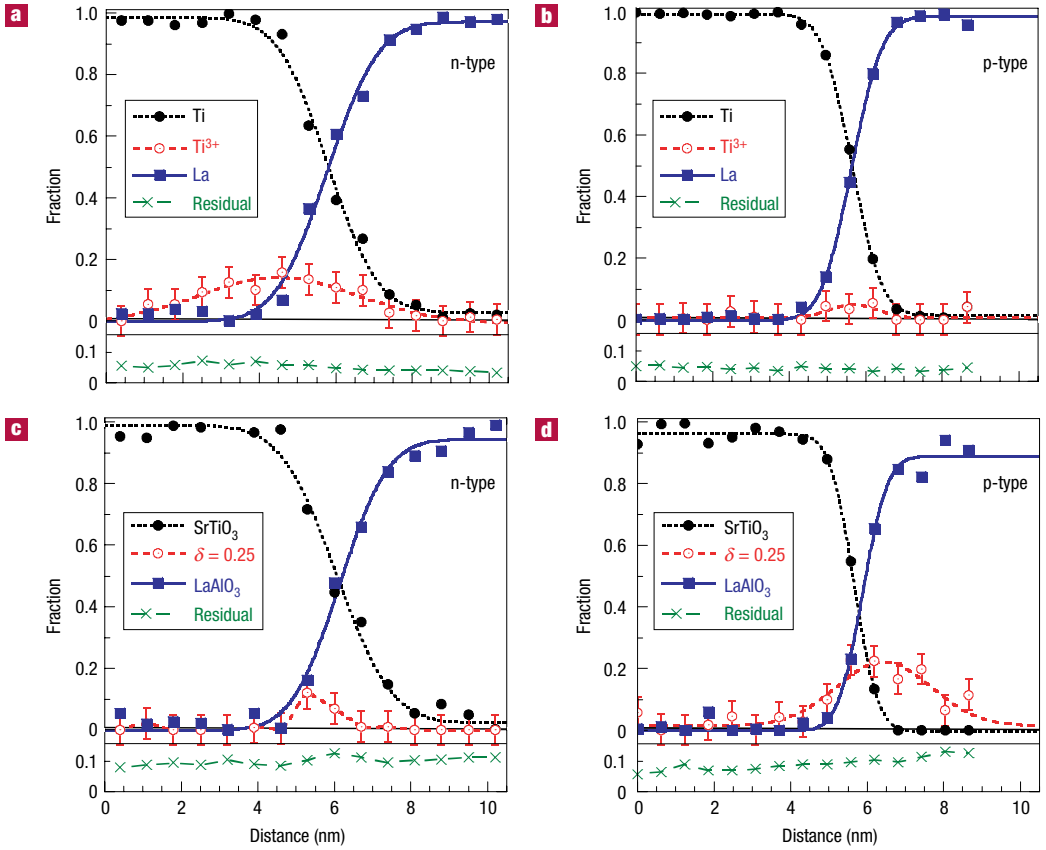

Figure 6 Chemical profiles of $LaAlO_3$ on (001) $SrTiO_3$ for both interface terminations. In each panel, the $SrTiO_3$ substrate is on the left and the $LaAlO_3$ on the right. **a**, AlO_2/LaO/TiO_2 interface showing the fractions of elemental Ti and La from the Ti-L and La-M edges, as well as the Ti^{3+} fraction determined from a least-squares fit to the Ti-L edge from Ti^{3+} and Ti^{4+} reference spectra. There is excess Ti^{3+} on the substrate side of the interface. **b**, Corresponding Ti and La EELS profiles for the AlO_2/SrO/TiO_2 interface, showing almost no excess Ti^{3+}. **c**, Fractional compositions from the least-squares fit to the O-K edge profile for the AlO_2/LaO/TiO_2 terminated interface, showing a net vacancy excess of $\delta = 0.1 \pm 0.04$. The labels are for the fits to the reference spectra as shown at the bottom of Fig. 5b. **d**, The O-K edge fractional composition (from Fig. 5b) for the AlO_2/SrO/TiO_2 interface showing a significant accumulation of excess vacancies ($\delta = 0.32 \pm 0.06$). The r.m.s. residual to the fits is shown below each plot.

point is that the interface with many oxygen vacancies has no excess electrons, whereas the interface with few oxygen vacancies has significant excess electrons. This is counter to the well-known role of oxygen vacancies in bulk oxides as electron donors, indicating that the origin and the function of the interface vacancies are completely different at the interface. This is bolstered by the fact that vacancies persist despite annealing in conditions far above those necessary to fill vacancies in thick $SrTiO_{3-\delta}$ films.

In comparing the valence profiles obtained from EELS with the simple model of half an electron per hole at the interface discussed in Fig. 1, the experimental data deviates from the model in two key respects. First, the electron are not fixed point charges, but delocalized in a screening cloud. This alters the size of the interface dipole but does not cause a divergence. Second, even though the net charge at the n-type interface is ~0.5 ($0.7 \pm 0.1\ e^-$, $0.2 \pm 0.08\ e^+$) there are more electrons than expected, which in turn are compensated for by slight oxygen vacancies, again altering the interface dipole.

In addition to the electrical asymmetry, why is there also an asymmetry in roughness? What we have ignored in this analysis so far is the delocalized electron cloud on the Ti sites at the AlO_2/LaO/TiO_2 interface. Spreading the electrons from a single plane to a few unit cells increases the interface dipole energy. This dipole can be reduced by exchanging Sr for La cations across the interface to produce a compensating dipole, that is, physically roughening the interface. (In general, an exchange of ions can only produce a dipole, but not add or remove a diverging potential.) Without a delocalized screening electron or hole charge at the AlO_2/SrO/TiO_2 interface, there is less need to compensate for cation-mixing across the interface. Furthermore, distribution of the oxygen vacancies can provide any necessary compensating dipole. Both the EELS profiles of Fig. 6 and the images of Fig. 2 show that the n-type AlO_2/LaO/TiO_2 interface is indeed rougher than the AlO_2/SrO/TiO_2 interface.

The presence of a small number of oxygen vacancies ($\delta = 0.1 \pm 0.04$) at the n-type interface (which should ideally have $\delta = 0$) suggests a mechanism to reduce the band offset while still avoiding a divergence. Adding extra vacancies and compensating electrons to keep the same net charge introduces an interface dipole that will shift the band offset. Consider the case where $\delta = 0.125$ and we place the missing one-in-eight O atoms in the SrO plane, that is, the interface structure is $SrO_{0.875}/Ti^{3.25+}O_2$/LaO/$AlO_2$. This gives 0.75 excess e^-/u.c. at the interface, but introduces no band offset (Fig. 7). In other words, the band offset can be tuned as a function of oxygen vacancy concentration, but with a price of adding electrons to the Ti conduction band at the interface.

A similar argument can be made for the p-type interface. The simplest interface of Fig. 1d would ideally have $\delta = 0.25$ and

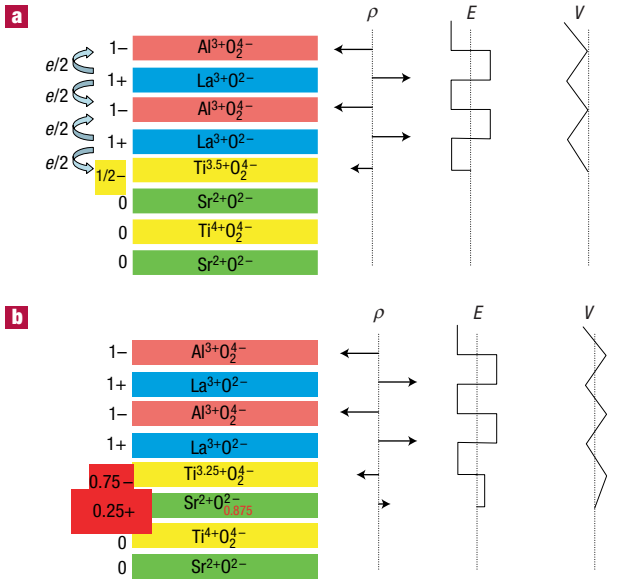

Figure 7 Tuning the band offset. a, The n-type interface of Fig. 1c where the average potential on the $LaAlO_3$ side is shifted by 0.46 V (the dipole shift assuming typical perovskite distances and performing the integral shown graphically). **b**, The band offset between $SrTiO_3$ and $LaAlO_3$ can be removed by adding an interface dipole composed of an extra 0.25 e^- on the interfacial TiO_2 layer, and an extra 0.125 oxygen vacancies on the next SrO layer. Overall, the net interface charge must remain at 0.5 to avoid a potential divergence.

one in four O atoms missing from the SrO plane, with no free electrons ($Ti^{4+}O_2/SrO_{0.75}/AlO_2/LaO$). The band offset can also be tuned for the p-type interface by removing O atoms and should have the same magnitude and opposite sign to the n-type case. The p-type interface with no band offset requires $\delta = 0.375$ and $Ti^{3.75+}O_2/SrO_{0.625}/AlO_2/LaO$, which gives 0.25 free electrons and three-in-eight missing O atoms in the SrO plane. The general case interpolates between $\delta = 0.25$ and 0.375. Experimentally, we find $\delta = 0.32 \pm 0.06$. The absence of a Ti^{3+} signal suggests the interface is closer to the ideal $\delta = 0.25$ (the lower end of the oxygen error range).

Controlling the interface termination layer lets us tune between insulator and conductor, trading chemical for electrical roughness. The band offset can be further adjusted by the oxygen-vacancy concentration, as discussed above, or by varying the cation ratio at the interface. Many oxide devices involve polar discontinuities at critical heterointerfaces such as in field-effect devices, tunnel junctions or ferroelectric/paraelectric interfaces. Our analysis suggests that the interface screening charges that result from the inevitable polar discontinuities are, at present, comparable to or larger than the largest polarizations achievable in field-effect devices, and comparable to the best ferroelectric polarizations. By changing the substrate termination layer, the screening charge could be substantially reduced, which in turn should markedly enhance the performance of these devices, possibly by orders of magnitude.

Received 17 October 2005; accepted 22 November 2005; published 22 January 2006.

References

1. Fong, D. D. *et al.* Ferroelectricity in ultrathin perovskite films. *Science* **304,** 1650–1653 (2004).
2. Junquera, J. & Ghosez, P. Critical thickness for ferroelectricity in perovskite ultrathin films. *Nature* **422,** 506–509 (2003).
3. Ahn, C. H., Triscone, J.-M. & Mannhart, J. Electric field effect in correlated oxide systems. *Nature* **424,** 1015–1018 (2004).
4. Ohtomo, A., Muller, D. A., Grazul, J. L. & Hwang, H. Y. Artificial charge-modulation in atomic-scale perovskite titanate superlattices. *Nature* **419,** 378–380 (2002).
5. Okamoto, S. & Millis, A. J. Electronic reconstruction at an interface between a Mott insulator and a band insulator. *Nature* **428,** 630–633 (2004).
6. Tung, R. Formation of an electric dipole at metal-semiconductor interfaces. *Phys. Rev. B* **64,** 205310 (2001).
7. McKee, R. A., Walker, F. J., Nardelli, M. B., Shelton, W. A. & Stocks, G. M. The interface phase and the Schottky barrier for a crystalline dielectric on silicon. *Science* **300,** 1726–1730 (2003).
8. Harrison, W. A., Kraut, E. A., Waldrop, J. R. & Grant, R. W. Polar heterojunction interfaces. *Phys. Rev. B* **18,** 4402–4410 (1978).
9. Baraff, G. A., Appelbaum, J. A. & Hamann, D. R. Self-consistent calculation of the electronic structure at an abrupt GaAs-Ge interface. *Phys. Rev. Lett.* **38,** 237–240 (1977).
10. Ohtomo, A. & Hwang, H. Y. A high-mobility electron gas at the $LaAlO_3/SrTiO_3$ heterointerface. *Nature* **427,** 423–426 (2004).
11. Klenov, D. O., Schlom, D. G., Li, H. & Stemmer, S. The interface between single crystalline (001) $LaAlO_3$ and (001) silicon. *Jpn J. Appl. Phys.* **44,** L617–L619 (2005).
12. Voyles, P. M., Muller, D. A., Grazul, J. L., Citrin, P. H. & Gossmann, H.-J. L. Atomic-scale imaging of individual dopant atoms and clusters in highly n-type bulk Si. *Nature* **416,** 826–829 (2002).
13. Muller, D. A., Nakagawa, N., Ohtomo, A., Grazul, J. L. & Hwang, H. Y. Atomic-scale imaging of nanoengineered oxygen vacancy profiles in $SrTiO_3$. *Nature* **430,** 657–661 (2004).
14. Batson, P. E. Simultaneous STEM imaging and electron energy-loss spectroscopy with atomic column sensitivity. *Nature* **366,** 727–728 (1993).
15. Varela, M. *et al.* Spectroscopic imaging of single atoms within a bulk solid. *Phys. Rev. Lett.* **92,** 095502 (2004).
16. Müller, J. E. & Wilkins, J. W. Band-structure approach to the x-ray spectra of metals. *Phys. Rev. B* **29,** 4331–4348 (1984).
17. Kirkland, E. J., Loane, R. F. & Silcox, J. Simulation of annular dark field STEM images using a modifed multislice method. *Ultramicroscopy* **23,** 77–96 (1987).
18. Abbate, M. *et al.* Soft-x-ray-absorption studies of the location of extra charges induced by substitution in controlled-valence materials. *Phys. Rev. B* **44,** 5419–5422 (1991).
19. Ohtomo, A., Muller, D. A., Grazul, J. L. & Hwang, H. Y. Epitaxial growth and electronic structure of $LaTiO_x$ films. *Appl. Phys. Lett.* **80,** 3922–3925 (2002).
20. Browning, N. D., Moltaji, H. O. & Buban, J. P. Investigation of three-dimensional grain-boundary structures in oxides through multiple-scattering analysis of spatially resolved electron-energy-loss spectra. *Phys. Rev. B* **58,** 8289–8300 (1998).
21. Francis, R. J., Moss, S. C. & Jacobson, A. J. X-ray truncation rod analysis of the reversible temperature-dependent [001] surface structure of $LaAlO_3$. *Phys. Rev. B* **64,** 235425 (2001).

Acknowledgements

We thank A. Ohtomo and M. Kawasaki for helpful discussions. This work was supported by the Mitsubishi Foundation, a Grant-in-Aid for Scientific Research on Priority Areas, and the US Office of Naval Research through the ONR EMMA MURI monitored by Colin Wood. N.N. acknowledges partial support from QPEC, Graduate School of Engineering, University of Tokyo. The Cornell Electron Microscope facilities have been supported by the NSF through the MRSEC and IMR programs. Correspondence and requests for materials should be addressed to D.A.M.

Competing financial interests

The authors declare that they have no competing financial interests.